

THE TILT OF THE HALO VELOCITY ELLIPSOID AND THE SHAPE OF THE MILKY WAY HALO

MARTIN C. SMITH,¹ N. WYN EVANS,¹ AND JIN H. AN^{2,3}

SUBMITTED TO *the Astrophysical Journal*

ABSTRACT

A sample of $\sim 1,800$ halo subdwarf stars with radial velocities and proper motions is assembled from Bramich et al.'s (2007) light-motion catalog. This is based on the repeated multi-band Sloan Digital Sky Survey photometric measurements in Stripe 82. Our sample of halo subdwarfs is extracted via a reduced proper motion diagram and distances are obtained using photometric parallaxes, thus giving full phase space information. The tilt of the velocity ellipsoid with respect to the spherical polar coordinate system is computed and found to be consistent with zero for two of the three tilt angles, and very small for the third. We prove that if the inner halo is in a steady-state and the triaxial velocity ellipsoid is everywhere aligned in spherical polar coordinates, then the potential must be spherically symmetric. The detectable, but very mild, misalignment with spherical polars is consistent with the perturbative effects of the Galactic disk on a spherical dark halo. Banana orbits are generated at the 1:1 resonance (in horizontal and vertical frequency) by the disk. They populate Galactic potentials at the typical radii of our subdwarf sample, along with the much more dominant short-axis tubes. However, on geometric grounds alone, the tilt cannot vanish for the banana orbits and this leads to a slight, but detectable, misalignment. We argue that the tilt of the stellar halo velocity ellipsoid therefore provides a hitherto largely neglected but important line of argument that the Milky Way's dark halo, which dominates the potential, must be nearly spherical.

Subject headings: subdwarfs — Galaxy: kinematics and dynamics — Galaxy: structure — Galaxy: halo

1. INTRODUCTION

The kinematics of any stellar population are often most conveniently described by its velocity dispersion tensor

$$\sigma_{ij}^2 \equiv \langle (v_i - \langle v_i \rangle)(v_j - \langle v_j \rangle) \rangle \quad (1)$$

where the subscript indices denote one of the orthogonal coordinate directions, and the angled brackets represent averaging over the phase space distribution function (see e.g., Binney & Tremaine 2008). The dispersion tensor is a symmetric second-rank tensor and so may always be diagonalized. The principal axes of the tensor then form a velocity ellipsoid, which need not be aligned with the coordinate directions. However, as already realized by Eddington (1915), if the gravity field is time-independent, then the alignment of the velocity ellipsoid is a powerful global probe of the gravitational potential.

The triaxiality of the local halo velocity ellipsoid is well-established (e.g., Woolley 1978; Chiba & Beers 2000; Gould 2003; Kepley et al. 2007; Smith et al. 2009). However, despite its importance, the alignment of the velocity ellipsoid of halo stars has received very little attention. Here, we construct an unprecedentedly large sample of $\sim 1,800$ halo subdwarf stars with known distances, radial velocities and proper motions in Sloan Digital Sky Survey (SDSS) Stripe 82. We find that the velocity dispersion tensor is anisotropic, with an align-

ment very close to that of the spherical polar coordinate axes.

If the velocity ellipsoid is exactly aligned radially everywhere, then the potential of the Milky Way is spherical in shape. The very mild misalignment that we detect is consistent with the influence of the Galactic disk on an underlying spherical Galactic halo potential.

2. THE SUBDWARF CATALOG

2.1. Sample Construction

We construct our sample of subdwarfs using data from the sixth SDSS data release (Adelman-McCarthy et al. 2008), in particular utilizing the light-motion catalog of Bramich et al. (2008). This is built from the multi-epoch, multi-band (u, g, r, i, z) photometry available for one of the SDSS equatorial stripes (Stripe 82) and covers ~ 250 deg² in the right ascension range $20^{\text{h}}7 < \alpha < 3^{\text{h}}3$ and in the declination range $|\delta| < 1^{\circ}26$. A full description of our subdwarf sample is given elsewhere (Smith et al. 2009). Here, we give a brief outline of the selection procedure.

The reduced proper motion is defined as

$$H_r = r + 5 \log_{10} \left(\frac{\mu}{\text{mas yr}^{-1}} \right) - 10, \quad (2)$$

where μ is the proper motion and r is the apparent magnitude in the r band, corrected for extinction using the maps of Schlegel et al. (1998). The reduced proper motion is useful because it is independent of distance, namely

$$H_r = M_r + 5 \log_{10} \left(\frac{v_{\text{tan}}}{4.74 \text{ km s}^{-1}} \right). \quad (3)$$

where M_r is the absolute magnitude in the r band and

¹ Institute of Astronomy, University of Cambridge, Madingley Road, Cambridge CB3 0HA, UK; msmith@ast.cam.ac.uk, nwe@ast.cam.ac.uk

² Dark Cosmology Centre, Niels Bohr Institute, University of Copenhagen, Juliane Maries Vej 30, DK-2100 Copenhagen Ø, Denmark jin@dark-cosmology.dk

³ Niels Bohr International Academy, Niels Bohr Institute, University of Copenhagen, Blegdamsvej 17, DK-2100 Copenhagen Ø, Denmark

v_{tan} is the tangential component of the velocity with respect to the line-of-sight between the Sun and the star. The reduced proper motion diagram is a plot of H_r versus color $g - i$, in which the populations of disk dwarf stars, white dwarfs and the halo subdwarfs are all separated (see e.g., Vidrih et al. 2007, who have already constructed a reduced proper motion diagram for Stripe 82 to isolate ultracool and halo white dwarfs).

Here, we are interested in selecting a clean sample of halo subdwarfs, and so we apply two pre-selection cuts in order to reduce the contamination.⁴ First, we only use stars that pass a quality cut such that uncertainties in the proper motion are smaller than 4 mas yr^{-1} . Secondly, the r magnitude of the star should be brighter than $r = 19.5$. This gives us a sample size of 372,811. The latter cut allows us to remove interlopers which may be at large distances and hence have small H_r despite having $\mu \sim 0 \text{ mas yr}^{-1}$. Neither cut introduces any kinematic bias. Note that we avoid cutting on μ directly in order to simplify our calculation of the detection efficiency.

In Figure 1, we show the reduced proper motion diagram. Owing to larger tangential velocities, the halo subdwarfs are clearly differentiated from the slower moving disk dwarfs. We estimate the location of the subdwarf boundary as

$$\begin{aligned} H_r &< 2.85(g - i) + 11.8 \text{ for } (g - i) \leq 2 \\ H_r &< 5.63(g - i) + 6.24 \text{ for } (g - i) > 2 \\ H_r &> 2.85(g - i) + 15.0 \text{ for } (g - i) \leq 1.3 \\ H_r &> 5.63(g - i) + 11.386 \text{ for } (g - i) > 1.3, \end{aligned} \quad (4)$$

and further clean the sample by rejecting all objects, which are within $\Delta H_r = 0.5$ of the boundary. These cuts result in a sample of 30,760 stars. We then cross-match with the output from the SDSS SEGUE spectral parameter pipeline (Lee et al. 2008). This provides us with the radial velocities for members of the subdwarf sample (with median error of 4.6 km s^{-1}), although it significantly reduces the sample size to 2,210 stars. The SEGUE spectroscopic target selection is a complicated function. Suffice it to say that, despite its complexity, it is believed to be free of any significant kinematic biases.

In order to recover the full six-dimensional phase-space information, we must determine the distance to each subdwarf. Ivezić et al. (2008) have already constructed a photometric parallax relation from SDSS observations of clusters, obtaining an intrinsic scatter of $\sim 0.2 \text{ mag}$ (Ivezić et al. 2008; Jurić et al. 2008; Sesar et al. 2008). Their parallax relation is also a function of $[\text{Fe}/\text{H}]$, which we obtain from the spectral parameter pipeline (with median error of 0.14 dex). Overall, the errors obtained from the Ivezić et al. (2008) relation are impressively small, aided by the high precision photometry from Bramich et al. (2008) – for our sample the median relative distance error is 10.1%.

In conjunction with the good accuracy on the Bramich et al. (2008) proper motions (less than 4 mas yr^{-1}), we are able to construct an unprece-

⁴ Possible contaminants such as white dwarfs, disk dwarfs or background giants can be considered to be negligible; Smith et al. (2009) conclude that the level of contamination for this sample is $\lesssim 1\%$.

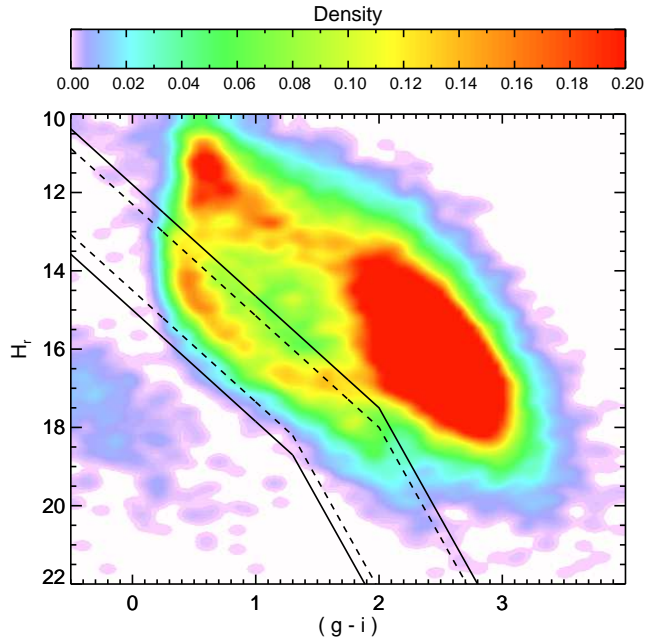


FIG. 1.— Reduced proper motion diagram of Stripe 82, where the color-scale corresponds to number density (scaled so that the peak is unity). The solid lines show the location of our subdwarf boundary, while the dashed lines show the region adopted to reduce contamination. To improve the clarity of the figure, we have incorporated a cut on the proper motion ($\mu > 30 \text{ mas yr}^{-1}$); the sample used throughout the paper has no such cut on μ . Note that the color-scale saturates at 20% of the peak density.

dedently large sample of halo subdwarfs with accurate positions and kinematics. The median error on each of our velocity components is $\sim 30\text{-}40 \text{ km s}^{-1}$. Restricting ourselves to subdwarfs with heliocentric distances less than 5 kpc gives a final sample of 1,782. These stars lie at Galactocentric cylindrical polar radii between 7 and 10 kpc, and at depths of 4.5 kpc or less below the Galactic plane.

2.2. Kinematic Bias Quantification

A drawback to our sample is that it is not kinematically unbiased, as the cut in the reduced proper motion diagram is implicitly a function of the kinematics. Therefore, we have to model and understand the effect of this if we are to investigate the distributions of velocities in our sample. Notice that the kinematic bias comes solely from our cut on the reduced proper motion H_r – which actually selects stars via their tangential velocity rather than their proper motion. This makes the task of quantifying the bias significantly easier since we do not need to make any assumptions about the underlying distance distribution (i.e., luminosity function).

We calculate our detection efficiency as follows. For each subdwarf in our final sample, we take the sky coordinates and create a mock sample of 50,000 fake stars. Then, for each mock star, we select M_r and $(g-i)$ at random from our observed distributions. Note that for each realization, *both* the magnitude and color are assigned from one star, i.e., we do not assign an absolute magnitude from one star and a color from another. We then select kinematics for each mock star using the Galactocentric halo velocity distributions from Képley et al. (2007)

but with no net rotation (Allende Prieto et al. 2006). To calculate v_{tan} from the Galactocentric velocities requires us to assign a distance to each mock star, which we do at random from the observed distribution. This means that the efficiency does have a dependence on the distance distribution. However, this dependence is very mild since equation (3) is a function of the tangential velocity rather than the proper motion. The efficiency is then given by the fraction of mock stars which pass our reduced proper motion cut.

In order to check whether our results are dependent on the assumed halo velocity distribution, we repeat the calculations using the values from Kepley et al. (2007), but now assuming a rotational velocity of the halo of $\sim 20 \text{ km s}^{-1}$ (in the direction of disk rotation). We find that uncertainties in the efficiency make little difference to the final determination of the tilts.

3. THE ALIGNMENT OF THE HALO VELOCITY ELLIPSOID

3.1. Method

With the efficiencies in hand, we can now calculate the misalignment of the velocity ellipsoid of the SDSS subdwarfs. To do this, we transform our subdwarf velocities into Galactocentric spherical polar coordinates: v_r is the radial velocity with respect to the center of the Galaxy, v_θ is the zenithal component measured from the North Galactic Pole, and v_ϕ is the azimuthal component measured such that the Galactic rotation has negative v_ϕ .

The misalignment from the spherical polar coordinate surfaces can then be described by the correlation coefficients and the tilt angles using the following formula

$$\text{Corr}[v_i, v_j] = \frac{\sigma_{ij}^2}{(\sigma_{ii}^2 \sigma_{jj}^2)^{1/2}} \quad (5)$$

and

$$\tan(2\alpha_{ij}) = \frac{2\sigma_{ij}^2}{\sigma_{ii}^2 - \sigma_{jj}^2}. \quad (6)$$

Here the tilt angle corresponds to the angle between the i -axis and the major axis of the ellipse formed by projecting the three dimensional velocity ellipsoid onto the ij -plane. (see e.g., Binney & Merrifield 1998, or Appendix A of this paper). We use the tilt angles to specify the orientation of the velocity ellipsoid, instead of alternatives such as the Euler angles because the former are a natural extension of the familiar two dimensional case and much easier to visualize than other options. See also recent examples of using the tilt angles in similar context by Dehnen & Binney (1998) and Siebert et al. (2008).

The measured sample covariance is due to both the true underlying covariance and the correlated measurement uncertainties, i.e.,

$$\text{Cov}_m[v_i, v_j] = \sigma_{ij}^2 + \text{Cov}[\delta v_i, \delta v_j], \quad (7)$$

where $\text{Cov}_m[v_i, v_j]$ is the covariance as measured from the sample and $\text{Cov}[\delta v_i, \delta v_j]$ is the covariance of the error distributions. To account for the detection efficiency, we also calculate the sample covariances weighted by the

inverse efficiency, e.g.,

$$\text{Cov}_m[v_i, v_j] = \frac{1}{W} \sum_{k=1}^N w_k (v_{i,k} - \langle v_{i,k} \rangle) (v_{j,k} - \langle v_{j,k} \rangle), \quad (8)$$

where

$$W = 1 - \sum_{k=1}^N w_k^2$$

and the summation is over the number of subdwarfs in our final sample. The weights w_k are proportional to reciprocal of the efficiency $\propto \epsilon_k^{-1}$ (normalized to unity such that $\sum_{k=1}^N w_k = 1$).

As indicated by equation (8), when the covariances are calculated we subtract the mean velocities, i.e., our results are not dependent on the assumed reference frame. However, as can be seen from Smith et al. (2009) our sample displays no significant net motion.

3.2. The Tilt Angles and Correlations

Let us first look at the tilt angles in the sample ignoring any stars with height $|z| < 1 \text{ kpc}$, so as to minimize (although not eliminate) any effect due to the Galactic disk potential. This gives us a sample of 1,532 subdwarfs. We find that the correlations and tilts are

$$\begin{aligned} \text{Corr}[v_r, v_\theta] &= 0.078 \pm 0.029, & \alpha_{r\theta} &= 3^\circ.4 \pm 1^\circ.3 \\ \text{Corr}[v_r, v_\phi] &= -0.028 \pm 0.039, & \alpha_{r\phi} &= -2^\circ.2 \pm 3^\circ.3 \\ \text{Corr}[v_\phi, v_\theta] &= -0.087 \pm 0.047, & \alpha_{\phi\theta} &= -37^\circ.4 \pm 20^\circ.4 \end{aligned} \quad (9)$$

where the errors are obtained using the bootstrap technique. We find no evidence of any clear tilt in the $\alpha_{r\phi}$ and $\alpha_{\phi\theta}$ terms. However, the tilt angle $\alpha_{r\theta}$ is measured to be non-zero at about 3- σ level, though it is still very small. The good alignment of the velocity ellipsoid in spherical polars is also apparent from the velocity distributions in the (v_r, v_θ) and (v_r, v_ϕ) planes illustrated in Figure 2, in which the dashed lines show the orientation of the tilts.

Note that the tilt angle $\alpha_{\phi\theta}$ is not well constrained since the dispersions in the two components are similar and the covariance is small. Hence, the calculation of $\alpha_{\phi\theta}$ involves the division of one small number by another small number, giving a large error. However, this term is not so important for the purpose of constraining the shape of the Galactic potential (see the next section).

The area of sky covered by the Stripe 82 catalogue is 249 deg^2 . It is reasonable to ask whether the velocity dispersion ellipsoid locally could have a different behaviour than that averaged over a larger region, especially as this effect has been observed recently in numerical simulations (Zemp et al. 2009). To study this, we investigate the variation in tilt as a function of height from the plane for $|z| \leq 4.5 \text{ kpc}$ in Figure 3. Neither of the tilt angles $\alpha_{r\theta}$ and $\alpha_{r\phi}$ show any significant trends. Although there are one or two isolated points at which the tilt angles lie at $\sim 1\text{-}\sigma$ from the mean, they are localized in longitude, indicative probably of kinematic substructure and streams which are expected in the stellar halo in hierarchical assembly models. The nature of the substructure in the SDSS subdwarfs is addressed in detail elsewhere (Smith et al. 2009). We have also carried out this test

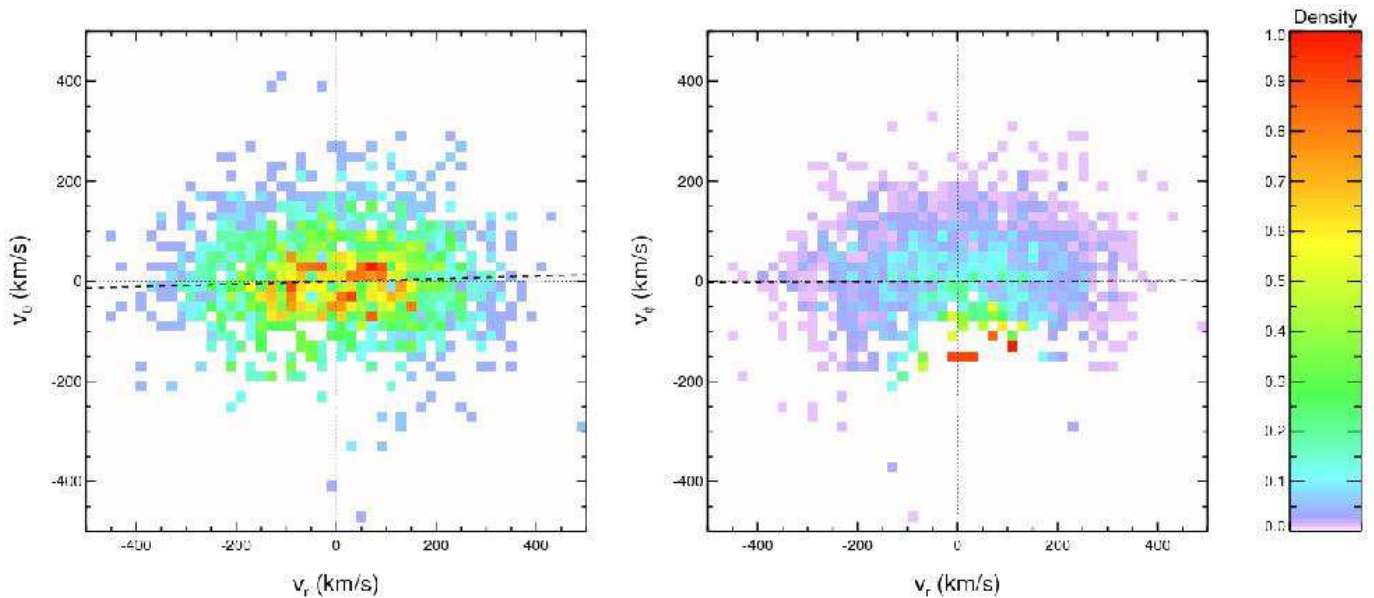


FIG. 2.— The efficiency corrected velocity distributions in the (v_r, v_θ) and (v_r, v_ϕ) planes for the sample of 1,532 subdwarfs with $1 \text{ kpc} < |z| < 4 \text{ kpc}$. The dashed lines show the orientation of the tilts. The apparent non-Gaussianity in the (v_r, v_ϕ) distribution is due to the variation of the efficiency correction across this plane; for certain regions of velocity space (particularly for $v_\phi \approx -200 \text{ km s}^{-1}$), our efficiency is low and hence the few stars that fall in this range are corrected by a large amount. This results in the narrow peaks in density in this figure, although when averaged over a larger area the density is consistent with a Gaussian distribution.

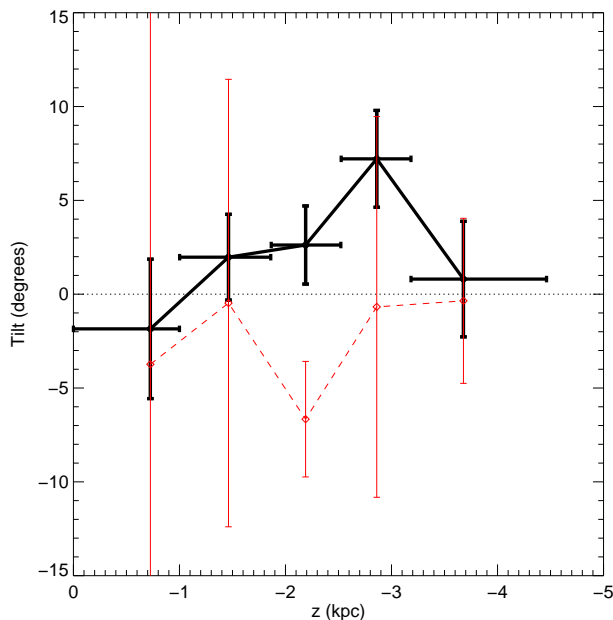


FIG. 3.— The variation of the tilt angles $\alpha_{r\theta}$ (black) and $\alpha_{r\phi}$ (red) as a function of height z from the Galactic plane. The vertical error bars are $1\text{-}\sigma$, whilst the horizontal error bars give the bin width. Although there are one or two locations where the deviation from the mean is greater than $1\text{-}\sigma$, there are no obvious trends discernible.

by splitting our sample into three according to right ascension, and find that the values of the tilt angles are consistent with those derived for the full sample.

4. DISCUSSION

4.1. Spherical Alignment

The alignment of the velocity ellipsoid of halo stars in spherical polar coordinate has substantial implications for the overall potential of the Galaxy. This constraint does not come from the Jeans equations, which merely require that the momentum flux balances the gravitational forces (see Evans, An & Walker (2009) or An & Evans (2009) for recent applications). Rather, the constraint comes from the deeper requirement that a phase space distribution function must exist. The theorem has been known for some time, although its widespread applicability has been obscured by the fact that Eddington (1915) and Chandrasekhar (1939) introduced unnecessary assumptions in its proof, as realized first by Lynden-Bell (1962).

Let us first note that there are a number of trivial ways that permit the velocity dispersion tensor to be aligned in spherical polar coordinates. The simplest is to ask for the distribution function to depend on energy E alone, in which case the velocity dispersion tensor is everywhere isotropic. Or, we could insist that the distribution function is given as $f = f(E, |\mathbf{L}|)$ in a spherical potential, or $f = f(E, L_z)$ in an axisymmetric potential. Here, \mathbf{L} is the angular momentum, whilst L_z is the component of \mathbf{L} that is parallel to the symmetry axis. All these options are not available to us because of the well-known and long established triaxiality of the velocity dispersion of halo stars with $\sigma_{rr}^2 > \sigma_{\phi\phi}^2 > \sigma_{\theta\theta}^2$ – see for example recent determinations by Kepley et al. (2007) or Smith et al. (2009).

To generate the observed triaxial anisotropy of the velocity dispersion tensor, the phase space distribution function must depend on at least three independent integrals of motion I_i , one of which may be chosen to be the same as the Hamiltonian, $I_1 = E(v_r^2, v_\theta^2, v_\phi^2; r, \theta, \phi)$.

Here, it is assumed that the reference frame is chosen such that there is no net bulk streaming motion, that is, $\langle v_r \rangle = \langle v_\theta \rangle = \langle v_\phi \rangle = 0$. Therefore, $\sigma_{rr}^2 = \langle v_r^2 \rangle$, $\sigma_{r\theta}^2 = \langle v_r v_\theta \rangle$ and so on. Accordingly, if the cross-terms $\langle v_r v_\theta \rangle$, and $\langle v_r v_\phi \rangle$ vanish everywhere, then any additional integrals of motion that isolate the distribution function must be even functions of v_r . This is equivalent to the statement that the v_r -dependence of the integrals is only through the square of the radial velocity component v_r^2 , and independent of the sign of v_r . Then, the second isolating integral I_2 can be recast as a globally defined function independent of v_r^2 using the energy integral, that is $I_2 = I_2(E; v_\theta, v_\phi; r, \theta, \phi)$. However, since I_2 is an integral of motion, its Poisson bracket with the Hamiltonian must vanish, from which it follows that I_2 also must be independent of r as well (Lynden-Bell 1962). Hence, the integral can always be cast in the form $I_2 = I_2(E; v_\theta, v_\phi; \theta, \phi)$ and so is completely independent of both r and (its conjugate momentum) v_r .

This implies that the radial coordinate in the Hamilton-Jacobi equation must separate and so the potential has to be of the form

$$\psi(r, \theta, \phi) = \psi_0(r) + \frac{\Psi(\theta, \phi)}{r^2}, \quad (10)$$

where ψ_0 and Ψ are arbitrary functions of the indicated arguments. In fact, by exactly the same line of reasoning applied to the third isolating integral I_3 , if $\langle v_\theta v_\phi \rangle$ also vanishes, then the potential has to have the form

$$\psi(r, \theta, \phi) = \psi_0(r) + \frac{\xi(\theta)}{r^2} + \frac{\zeta(\phi)}{r^2 \sin^2 \theta}, \quad (11)$$

although this is a stronger result than we will need here.

If the potential has the form (10), then Poisson's equation implies that the total density of stars and dark matter is

$$\rho(r, \theta, \phi) = \rho_0(r) + \frac{\Omega(\theta, \phi)}{4\pi G r^4}, \quad (12)$$

where

$$\rho_0 = \frac{1}{4\pi G r^2} \frac{d}{dr} \left(r^2 \frac{d\psi_0}{dr} \right)$$

$$\Omega = \frac{1}{\sin \theta} \frac{\partial}{\partial \theta} \left(\sin \theta \frac{\partial \Psi}{\partial \theta} \right) + \frac{1}{\sin^2 \theta} \frac{\partial^2 \Psi}{\partial \phi^2}.$$

That is to say, the dipole potential is necessarily associated with an astrophysically unrealistic density cusp diverging as r^{-4} unless $\Omega = 0$. Consequently, we have $\Psi = 0$.⁵ This leaves us with the theorem that:

If a steady state stellar population has a non-degenerate (i.e. triaxial) velocity dispersion tensor whose eigenvectors are everywhere aligned in spherical polar coordinates, then the underlying gravitational potential must be spherically symmetric.

This theorem is implicit in Lynden-Bell (1962), whereas restricted versions were known to Eddington (1915) and

Chandrasekhar (1939). In fact, from the preceding proof, the crux of the result lies in the existence of the second integral that forces the separation of the radial part of the Hamilton-Jacobi equation, and the presence of the third integral is of a secondary importance. Hence, the theorem can be relaxed somewhat:

If the potential is non-singular, it is a sufficient condition for a spherical symmetry that one of the non-degenerate eigenvectors of the velocity dispersion tensor is aligned radially everywhere.

This follows, as spherical symmetry is guaranteed for non-singular potentials once the radial part of the Hamilton-Jacobi equation can be separated off.

Of course, spherical alignment of the velocity dispersion tensor does not imply that the stellar density itself is spherically symmetric. In fact, many investigators have already found that $\sigma_{\theta\theta}^2 \neq \sigma_{\phi\phi}^2$ for samples of halo stars (e.g., Gould 2003; Kepley et al. 2007; Smith et al. 2009), which implies that the stellar halo has a density distribution that is flattened or triaxial even though the gravity field is nearly spherical. This is the case, for example, in the models presented by White (1985), Arnold (1990), and Evans, Hafner & de Zeeuw (1997), in which the phase space distribution function depends on energy and the all three components of angular momentum, $f = f(E, \mathbf{L})$.

4.2. Nearly Spherical Alignment

The tilt angles $\alpha_{r\phi}$ and $\alpha_{\phi\theta}$ are consistent with zero, but our results give a very small, but non-zero measurement of the tilt angle $\alpha_{r\theta}$ (at the 3- σ level). In an exactly spherical potential, the $\langle v_r v_\theta \rangle$ cross-term and hence $\alpha_{r\theta}$ must vanish. However, even if the dark halo is spherical, the Galactic potential is not spherical due to the influence of the bulge and the disk. Of course, at the distances probed by our sample of SDSS subdwarfs, it is the halo that dominates the gravitational potential, whilst the disk gives the main perturbation.

The main consequence of the disk is to convert the planar rosette orbits of a spherical potential into the short-axis tube orbits of a mildly oblate potential. However, in typical axisymmetric Galactic potentials, the key 1:1 resonance (in cylindrical coordinates R and z) also occurs at Galactocentric radii between 2 and 10 kpc, causing the axial orbits to become unstable to out-of-plane perturbations, and siring the family of banana or saucer orbits (see e.g., Pfenniger 1984; Miralda-Escudé & Schwarzschild 1989; Schwarzschild 1993; Evans 1994; Binney & Tremaine 2008, Section 3.7.3). It is to these two orbital families – the short-axis tubes and the bananas – that our SDSS subdwarfs will belong.

We can confirm this by computing orbits in the Milky Way potential of Fellhauer et al. (2006), which comprises a spherical isothermal halo and a Miyamoto-Nagai disk. Our initial conditions were chosen as follows: since the potential is axisymmetric, we start our orbits off from a location $x = 8$ kpc, $y = 0$ kpc and with z distributed uniformly from -1 to -4 kpc (which is a reasonable approximation of our observed distribution). Our initial velocities were chosen according to the trivariate ellipsoidal Gaussian $\sigma_r = 142$ km s⁻¹, $\sigma_\phi = 81$ km s⁻¹, and

⁵ Mathematically, Ψ may be any combination of spherical harmonics $Y_m^l(\theta, \phi)$ with $l = 1$. However, there must not be any physical source for the pure-dipole gravitational field, and so Ψ may be set to zero by appropriate choice of the coordinate origin.

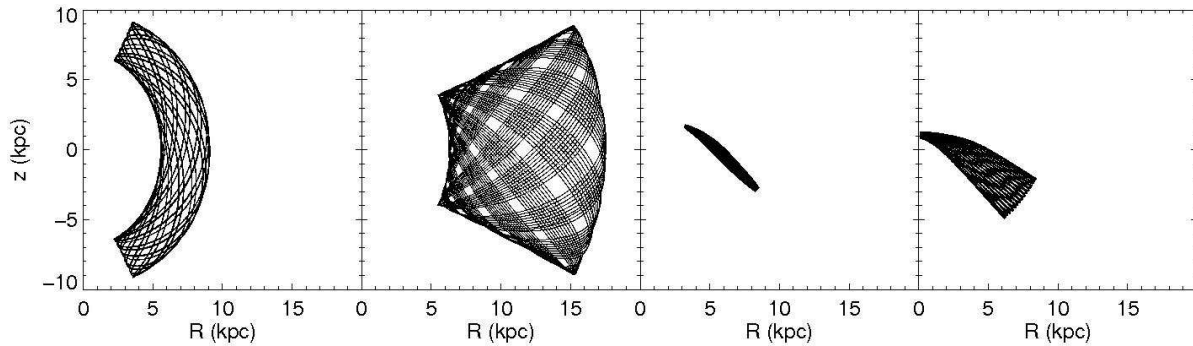


FIG. 4.— Cross-sections in the meridional plane of typical orbits of the SDSS subdwarfs; leftmost two panels showing thin and thick tube orbits, rightmost two panels showing banana or saucer orbits.

$\sigma_\theta = 77 \text{ km s}^{-1}$, i.e., according to the values derived for our observed sample of halo subdwarfs by Smith et al. (2009). This is of course not a *bona fide* distribution function, but just a convenient sampling function to scan phase space. The orbits were calculated using a fourth order Runge-Kutta method with a time-step of 0.1 Myr, which results in a fractional energy change of better than 10^{-6} over a typical orbital period of ~ 200 Myr. The orbits so produced are indeed predominantly short-axis tubes ($\sim 80\%$), but with a reasonable mixture of banana orbits ($\sim 20\%$). Some examples are illustrated in the panels of Figure 4.

It is immediately apparent on geometrical grounds that the banana orbits can only give positive contributions to $\langle v_r v_\theta \rangle$. By contrast, the short-axis tubes can yield both positive and negative contributions. Hence, the effect of the Galactic disk is to create a family of orbits for which the tilt term $\sigma_{r\theta}^2$ cannot exactly vanish.

In fact, it is easy to bolster this geometric argument with a quantitative calculation. Using our sampling function, we generated 96 initial conditions and integrated the orbits for 1 Tyr, recording the velocities each time a test particle returned to its initial position (defined in practice to within a spherical volume of 300 pc radius). The enormous timescale is to maximize the number of times a particle returns to its initial position, so that $\sigma_{r\theta}^2$ for the orbit can be calculated as accurately as possible. Then, we average the resulting values of $\sigma_{r\theta}^2$ for every crossing and for all of our orbits. This gives $\langle v_r v_\theta \rangle = 690 \text{ km}^2 \text{ s}^{-2}$, which is very comparable to our observed covariance of $893 \pm 335 \text{ km}^2 \text{ s}^{-2}$.

However, if we divide our orbits into banana and short-axis tubes (banana orbits are defined as those which are asymmetric about $z = 0$ or the Galactic plane) and recalculate the average $\sigma_{r\theta}^2$, then we find that the 19 banana orbits have $\langle v_r v_\theta \rangle = 1740 \text{ km}^2 \text{ s}^{-2}$, while the remaining 77 short-axis tube orbits have $\langle v_r v_\theta \rangle = -140 \text{ km}^2 \text{ s}^{-2}$. The banana orbits indeed contribute almost all of the effect. As a check, if we repeat this procedure in a spherical potential (i.e., without the Galactic disk), we indeed find that $\langle v_r v_\theta \rangle$ is consistent with zero, as it should be.

A very mild misalignment in the velocity ellipsoid of the SDSS subdwarfs with respect to spherical polar coordinates is therefore naturally explained by the effects of the Galactic disk.

5. CONCLUSIONS

The Milky Way’s dark halo dominates the gravity field, and different datasets have yielded very different values for its flattening. For example, analyses of the variation of the thickness of the Galaxy’s gas layer with radius point to an oblate halo with axis ratio $q \sim 0.7$ (Olling & Merrifield 2001). This is consistent with the typical values of halo flattening measured for some external galaxies, using the dynamics of polar rings or the shapes of the isophotes of the X-ray emission for early-type galaxies. On the other hand, Fellhauer et al. (2006) reached the very different conclusion that the dark halo of our own Galaxy must be very close to spherical, based on dynamical modeling of the bifurcation in the Sagittarius stream. Finally, Helmi (2004) used the kinematic data of stars in the leading arm of the Sagittarius to argue that the dark halo is prolate.

Here, we have drawn attention to another – somewhat neglected – probe of the shape of the dark halo, namely the tilt of the velocity ellipsoid of halo stars. In a pure spherical halo, the velocity ellipsoid of any tracer population – regardless of whether its density distribution is flattened or triaxial – must be aligned in the spherical polar coordinate system. By contrast, the behavior of the velocity ellipsoid in flattened halos is much more varied. For example, Levison & Richstone (1985a,b) constructed a number of halo models with ellipticities between 0.3 and 0.7 using the Schwarzschild method. They show numerous plots of the behavior of the velocity ellipsoid, from which it is apparent that it deviates, often very strongly, from spherical polar alignment.

In this paper, the tilt of the velocity ellipsoid of the Milky Way halo stars has been measured using an unprecedentedly large sample of $\sim 1,800$ halo subdwarfs extracted from Bramich et al.’s (2008) light-motion catalog, itself based on the repeated Sloan Digital Sky Survey observations of Stripe 82. We find that the velocity ellipsoid of the halo subdwarfs is very closely aligned with the spherical polar coordinate system. In particular, two of the tilt angles are consistent with zero, whereas the final tilt angle – corresponding to the $\langle v_r v_\theta \rangle$ term – is very small. We have shown that this effect is consistent with the influence of the Galactic disk, which must cause a mild asphericity in the total potential even if the dark halo itself is spherical. This asphericity gives rise to a family of orbits, the banana or saucer orbits, which are typically represented in samples of stars at the locations of the SDSS subdwarfs. On geometric grounds alone,

$\langle v_r v_\theta \rangle$ does not exactly vanish for banana orbits, and so their small admixture causes a very mild misalignment.

Our argument here is open to the criticism that we have not shown that the velocity dispersion tensor is aligned everywhere in spherical polar coordinates. We have merely shown that the alignment is very close to spherical polars for halo subdwarfs at heliocentric distances of $\lesssim 5$ kpc along the ~ 250 deg² covered by SDSS Stripe 82. Nonetheless, this is still a striking and unexpected result over a swathe of Galactic locations that provides a new line of attack on the awkward question of the shape of the Milky Way's dark halo. It would be very interesting to extend our results to samples of halo stars in different directions. This is particular the case for high latitude samples of halo stars, for which any effects due to the Galactic disk are negligible, and so for which alignment with the spherical polar coordinate system should be perfect.

The authors wish to thank V. Belokurov, P. Hewett, M. Jurić and an anonymous referee for advice and guidance. The Dark Cosmology Centre is funded by the Danish National Research Foundation. MCS acknowledges support from the STFC-funded ‘‘Galaxy Formation and Evolution’’ program at the Institute of Astronomy, University of Cambridge.

Funding for the SDSS and SDSS-II has been provided by the Alfred P. Sloan Foundation, the Participating Institutions, the National Science Foundation, the U.S. Department of Energy, the National Aeronautics and Space Administration, the Japanese Monbukagakusho, the Max Planck Society, and the Higher Education Funding Council for England. The SDSS Web Site is <http://www.sdss.org/>.

The SDSS is managed by the Astrophysical Research Consortium for the Participating Institutions. The Participating Institutions are the American Museum of Natural History, Astrophysical Institute Potsdam, University of Basel, Cambridge University, Case Western Reserve University, University of Chicago, Drexel University, Fermilab, the Institute for Advanced Study, the Japan Participation Group, Johns Hopkins University, the Joint Institute for Nuclear Astrophysics, the Kavli Institute for Particle Astrophysics and Cosmology, the Korean Scientist Group, the Chinese Academy of Sciences (LAMOST), Los Alamos National Laboratory, the Max-Planck-Institute for Astronomy (MPIA), the Max-Planck-Institute for Astrophysics (MPA), New Mexico State University, Ohio State University, University of Pittsburgh, University of Portsmouth, Princeton University, the United States Naval Observatory, and the University of Washington.

REFERENCES

- Adelman-McCarthy, J., et al. 2008, *ApJS*, 175, 297
 An, J.H., Evans, N.W., 2009, *ApJ*, submitted
 Arnold, R. 1990, *MNRAS*, 244, 465
 Allende Prieto, C., Beers, T. C., Wilhelm, R., Newberg, H. J., Rockosi, C. M., Yanny, B., & Lee, Y. S. 2006, *ApJ*, 636, 804
 Binney J., & Merrifield M. 1998, *Galactic Astronomy* (Princeton: Princeton University Press)
 Binney, J., & Tremaine S. 2008, *Galactic Dynamics*, 2nd ed, (Princeton: Princeton University Press)
 Bramich, D. M., et al. 2008, *MNRAS*, 386, 887
 Chandrasekhar, S. 1939, *ApJ*, 90, 1
 Chiba M., & Beers T. C. 2000, *AJ*, 119, 2843
 Dehnen, W., & Binney, J. J. 1998, *MNRAS*, 298, 387
 Eddington, A. S. 1915, *MNRAS*, 76, 37
 Evans, N. W. 1994, *MNRAS*, 267, 333
 Evans, N. W., Hafner R. M., & de Zeeuw, P. T. 1997, *MNRAS*, 286, 315
 Evans, N. W., An, J., & Walker, M. 2009, *MNRAS*, 393, L50
 Fellhauer, M., et al. 2006, *ApJ*, 651, 167
 Gould, A. 2003, *ApJ*, 583, 765
 Helmi, A. 2004, *ApJ*, 610, L97
 Ivezić, Ž., et al. 2008, *ApJ*, 684, 287
 Jurić, M., et al. 2008, *ApJ*, 673, 864
 Kewley, A. A., et al. 2007, *AJ*, 134, 1579
 Lee, Y. S., et al. 2008, *AJ*, 136, 2022
 Levison, H., & Richstone, D. 1985a, *ApJ*, 295, 340
 Levison, H., & Richstone, D. 1985b, *ApJ*, 295, 349
 Lynden-Bell, D. 1962, *MNRAS*, 124, 95
 Miralda-Escudé, J., & Schwarzschild, M. 1989, *ApJ*, 339, 751
 Olling, R. P., & Merrifield, M. R. 2001, *MNRAS*, 326, 164
 Pfenniger, D., 1984, *A&A*, 134, 373
 Schwarzschild, M. 1993, *ApJ*, 409, 563
 Schlegel, D. J., Finkbeiner, D. P., & Davis, M. 1998, *ApJ*, 500, 525
 Sesar, B., Ivezić, Ž., & Jurić, M. 2008, *ApJ*, 689, 1244
 Siebert, A., et al. 2008, *MNRAS*, 391, 793
 Smith, M. C., et al. 2009, *MNRAS*, submitted
 Vidrih, S., et al. 2007, *MNRAS*, 382, 515
 White, S. D. M. 1985, *ApJ*, 294, L99
 Woolley, R., 1978, *MNRAS*, 184, 311
 Zemp M., Diemand J., Kuhlen M., Madau P., Moore B., Potter D., Steidel J., & Widrow L., 2008, *ApJ*, submitted (arXiv 0812.2033)

APPENDIX

THE TILT ANGLES AND THE VELOCITY ELLIPSOID

After the mean motion has been subtracted, the velocity dispersion is

$$\sigma_{ij}^2 = \int d^3\mathbf{v} v_i v_j f. \quad (\text{A1})$$

If we consider a coordinate transformation $v_{i'} = \Lambda_{i'j} v_j$ (henceforth the summation convention for repeated indices is used) in velocity space given by a matrix in $\text{SO}(3)$, it is straightforward to verify that the velocity dispersion transforms as a component of a tensor, i.e.,

$$\sigma_{i'j'}^2 = \int d^3\mathbf{v} v_{i'} v_{j'} f = \int d^3\mathbf{v} (\Lambda_{i'k} v_k) (\Lambda_{j'l} v_l) f = \Lambda_{i'k} \Lambda_{j'l} \sigma_{kl}^2 \quad (\text{A2})$$

where the Jacobian relating the coordinate transformation is unity.

Note from the definition that the velocity dispersion tensor is symmetric and its three eigenvalues are all positive definite. Hence, it is also invertible. Let $(\zeta_{ij}^2) = (\sigma_{ij}^2)^{-1}$ be the matrix inverse of the velocity dispersion tensor. The

velocity ellipsoid is then defined to be a quadric surface in velocity space

$$\zeta_{ij}^2 v_i v_j = 1. \quad (\text{A3})$$

Next, from the rule involving the inversion of the product of matrices and the fact $\Lambda_{i'j}$ is an orthogonal matrix (i.e., $\Lambda_{ij'}^{-1} = \Lambda_{j'i}$), it is clear that ζ_{ij}^2 also transforms as a tensor, that is to say, $\zeta_{i'j'}^2 = \Lambda_{i'k} \Lambda_{j'l} \zeta_{kl}^2$. Then,

$$\zeta_{ij}^2 v_i v_j = \zeta_{ij}^2 \Lambda_{ik'}^{-1} v_{k'} \Lambda_{j'l}^{-1} v_{l'} = \Lambda_{k'i} \Lambda_{l'j} \zeta_{ij}^2 v_{k'} v_{l'} = \zeta_{k'l}^2 v_{k'} v_{l'},$$

and thus the equation of the velocity ellipsoid is form-invariant under orthogonal coordinate transformations. If the primed coordinate axes are chosen to be aligned to the principal axes of the velocity ellipsoid, the equation of the ellipsoid in the primed coordinate is in the canonical form. It then follows that $\zeta_{i'j'}^2$ and subsequently $\sigma_{i'j'}^2$ are diagonalized in the same primed coordinate system. In other words, the coordinate transformation to the system with the basis set given by the principal axes of the velocity ellipsoid is identical to the one diagonalizing the velocity dispersion tensor.

Next, we consider the projection of the velocity ellipsoid. Here, we suppose that the projection is onto the $v_x v_y$ -plane, although the other two follow basically the same procedure. Let us think of a line with fixed (v_x, v_y) but with varying v_z . If (v_x, v_y) falls within the projection of the ellipsoid, the line intersects the ellipsoid in two points. On the other hand, if the point (v_x, v_y) is outside the projection in the $v_x v_y$ -plane, the line does not cross the ellipsoid. Following similar logic, we find that the point (v_x, v_y) is on the projection of the ellipsoid in the $v_x v_y$ -plane if the line running perpendicular to the plane through the given point is a tangent to the ellipsoid. Now, if the equation of the ellipsoid is considered as a quadratic equation for z given fixed (v_x, v_y) , the preceding argument indicates that setting its discriminant to be zero defines the equation of the projection in the $v_x v_y$ -plane. Therefore, we find the equation of the projection of the velocity ellipsoid onto the $v_x v_y$ -plane;

$$C_{yy} v_x^2 - 2C_{xy} v_x v_y + C_{xx} v_y^2 = \zeta_{zz}^2, \quad (\text{A4})$$

where C_{xx} , C_{xy} , and C_{yy} are the matrix cofactors of ζ_{xx}^2 , ζ_{xy}^2 , and ζ_{yy}^2 , respectively. This traces an ellipse in $v_x v_y$ -plane.

The projected velocity dispersion tensor corresponding to this ellipse may be defined analogously to the 3-d case. After some algebra, we find that

$$\begin{pmatrix} C_{yy}/\zeta_{zz}^2 & -C_{xy}/\zeta_{zz}^2 \\ -C_{xy}/\zeta_{zz}^2 & C_{xx}/\zeta_{zz}^2 \end{pmatrix}^{-1} = \frac{1}{D} \begin{pmatrix} C_{xx} & C_{xy} \\ C_{xy} & C_{yy} \end{pmatrix} = \begin{pmatrix} \sigma_{xx}^2 & \sigma_{xy}^2 \\ \sigma_{xy}^2 & \sigma_{yy}^2 \end{pmatrix} \quad (\text{A5})$$

where $D = |\zeta_{ij}^2|$ is the matrix determinant of (ζ_{ij}^2) . In other words, the projection of the velocity ellipsoid onto the $v_x v_y$ -plane is the same as the 2-d velocity ‘ellipsoid’ calculated with the 2×2 (v_x, v_y) -submatrix of the original 3×3 velocity dispersion matrix. Consequently, the tilt angle defined as in equation (6) is the same as the angle between the principal axis of the ellipse that is the projection of the velocity ellipsoid onto the ij -plane and the coordinate axis. We note however that this is not the same as the angle between the coordinate axis and the projection of the principal axis of the velocity ellipsoid onto the same plane – that is to say, the principal axis of the velocity ellipsoid is not necessarily projected into the principal axis of the projected ellipse.